

# A Preliminary Comparison Between Compressive Sampling and Anisotropic Mesh-based Image Representation

Xianping Li <sup>\*</sup>      Teresa Wu <sup>†</sup>

## Abstract

Compressed sensing (CS) has become a popular field in the last two decades to represent and reconstruct a sparse signal with much fewer samples than the signal itself. Although regular images are not sparse on their own, many can be sparsely represented in wavelet transform domain. Therefore, CS has also been widely applied to represent digital images. However, an alternative approach, adaptive sampling such as mesh-based image representation (MbIR), has not attracted as much attention. MbIR works directly on image pixels and represents the image with fewer points using a triangular mesh. In this paper, we perform a preliminary comparison between the CS and a recently developed MbIR method, AMA representation. The results demonstrate that, at the same sample density, AMA representation can provide better reconstruction quality than CS based on the tested algorithms. Further investigation with recent algorithms is needed to perform a thorough comparison.

**Keywords.** Compressive sampling, mesh-based image representation, AMA representation, PSNR, Structural similarity index measure

## 1 Introduction

Compressive sampling (CS, also known as compressive sensing, compressed sensing, sparse sampling) has become popular in signal processing for the last two decades, and numerous research has been performed in this field. The literature is superabundant to be listed entirely, and only a few are referred here [1, 2, 3, 4, 5, 6, 7, 8]. CS has been applied to computed tomography (CT) [9, 10] and MRI [11, 12, 13] reconstructions to improve the acquisition speed. It has also been applied to represent digital images obtained from different sources [14, 15], although many images are not sparse on their own.

In this paper, we focus on the representation of digital images from different sources, such as digital cameras, remote sensing images, as well as MR images that have already been obtained/reconstructed.

---

<sup>\*</sup>College of Integrative Sciences and Arts, Arizona State University, Mesa, AZ 85212, U.S.A. (*Xianping.Li@asu.edu*)

<sup>†</sup>School of Computing, Informatics, Decision Systems Engineering, Arizona State University, Tempe, AZ 85281, U.S.A. (*Teresa.Wu@asu.edu*)

In many processing tasks of those images, it is also desirable to represent the images with fewer pixels to reduce the image size and improve processing efficiency. One example is image segmentation via a variational approach. In those cases, we need to work on the image pixels directly.

Adaptive sampling based on image pixels, especially, triangular mesh-based image representation (MbIR), has recently gained much interest, although not as much as compressive sampling that works on transformed domain. Some publications about MbIR are listed here [16, 17, 18, 19, 20, 21, 22, 23, 24, 25]. In particular, Li developed the anisotropic mesh adaptation for image representation framework (AMA representation) in [25] that provides better representation quality with reasonable computational cost than other MbIR methods.

Although CS is much more popular than MbIR, it is not clear if it performs better than MbIR in terms of reconstruction quality, especially for natural images that are not sparse on their own. This paper aims to perform a preliminary comparison between CS and MbIR for digital images from different sources and provide guidance for further research efforts in the area of image representation.

The rest of the paper is organized as follows. Section 2 gives a brief description of compressive sampling (CS) as well as mesh-based image representation. Some CS algorithms and a recently developed MbIR method, anisotropic mesh adaptation for image representation (AMA representation), are introduced. Section 3 describes the comparison metrics and presents the results for images of different styles and resolutions. A short conclusion is given in Section 4.

## 2 Compressive sampling and mesh-based image representation

In this section, we briefly introduce the two image representation approaches: compressive sampling and adaptive sampling, in particular, anisotropic mesh adaptation for image representation (AMA representation) that is a recently developed anisotropic mesh-based image representation framework.

### 2.1 Compressive sampling

The key idea of compressive sampling (CS) is the sparsity of the signal that needs to be reconstructed. A signal is called sparse if most of its components are zero. It is possible to represent a sparse signal using a small number of measurements and reconstruct it by solving an underdetermined linear system. By reducing the sampling rate, CS can improve the signal acquisition and transmission speed and reduce hardware requirements for sensors. It takes more computational effort during reconstruction on the receiver side.

Let  $\vec{x} \in \mathbb{C}^N$  be a sparse vector needs to be reconstructed from the underdetermined measurements  $\vec{x}_{meas} = A\vec{x} \in \mathbb{C}^m$  with  $m \ll N$ . Then there are two key steps in CS.

1. Design the measurement (also called sensing) matrix  $A \in \mathbb{C}^{m \times N}$  so that as much intrinsic information will contribute to the reconstruction.
2. Solve  $\vec{x}$  from the underdetermined linear system  $\vec{x}_{meas} = A\vec{x}$  with balance of efficiency and accuracy.

For image representation purpose, we convert the 2D images into a vector  $\vec{x} \in \mathbb{R}^N$ , which serves as the ground truth. Although  $\vec{x}$  may not be sparse on its own, it can be sparse in wavelet or Fourier domain. Thus,  $m(\ll N)$  sample points are randomly chosen from  $\vec{x}$  in wavelet or Fourier domain. Then a random matrix  $A$  of the corresponding size is generated according to the sample points. The measurement data is simulated by multiplying  $A$  and  $\vec{x}$  as  $\vec{x}_{meas} = A\vec{x} \in \mathbb{R}^m$ . The ratio  $m/N$  is denoted as the *sample density* of the representation.

For the reconstruction step, we consider two methods here. One is to solve the  $l_1$ -minimization problem by using the log-barrier algorithm, and the  $l_1$ -MAGIC package [26] (written in MATLAB) is used for the computations. The other is the iterative soft thresholding algorithm (ISTA), and the *pit* package [27] (written in Python) is used for the computations. Minor modifications of the program codes have been made to display the reconstructed image as well as compute the quality of reconstruction.

## 2.2 AMA representation

Different from CS, adaptive sampling works directly on image pixels. The idea is to choose the essential pixels of the image and discard non-important ones. Various approaches, especially mesh-based image representation methods, have been developed since the 1990s. Here, we briefly introduce the recently developed AMA representation framework [25] that consists of four key steps.

1. Generate an initial triangular mesh based on the desired sample density. The sample density determines the number of vertices in the mesh. Delaunay triangulation can be used to generate the initial mesh.
2. Assign values to mesh vertices from original image grey values using linear finite element interpolation and compute the user-defined metric tensor  $\mathbb{M}$  on the mesh.
3. Adapt the mesh to be a quasi- $\mathbb{M}$ -uniform mesh that almost fits the provided metric tensor  $\mathbb{M}$ .
4. Reconstruct the image using the final adaptive mesh with finite element interpolation for triangles.

Steps 2 and 3 can be repeated a few times in order to obtain a good adaptive mesh, which is the part that takes most computational resources in this framework.

Li also proposed the GPRAMA method in [25] that combines the greedy-point-removal algorithm with AMA representation using mesh patching techniques. GPRAMA can provide better representation quality than AMA but is computationally more expensive due to the greedy-point-removal procedure. As a preliminary investigation, we only consider AMA representation in this paper.

## 3 Comparison results

In this section, we present the results obtained for eight images of different styles and resolutions. The parameter values for CS algorithms are taken from the packages as default. For AMA representation, the anisotropic metric tensor  $\mathbb{M}_{aniso}$  (Eq. (8) in [25]) is used.

In  $l_1$ -MAGIC package, the *CS\_tveq()* function solves a total variation minimization problem with equality constraints. For the tested images, this function provides better reconstruction quality as well as takes less time than *CS\_tvqc()* function that solves a total variation minimization problem with quadratic constraints. Although *CS\_tvqc* with quantization runs faster than *CS\_tveq()*, the reconstruction quality is worse. Thus, only the results obtained from *CS\_tveq()* function are presented in this paper and denoted as TVeq.

The results obtained from the Python package *pit* using the iterative soft thresholding algorithm are denoted as ISTA. And the results obtained from AMA representation are denoted as AMA.

### 3.1 Comparison metrics

To compare the quality of the reconstruction from different approaches, we consider two commonly used metrics: peak-signal-to-noise-ratio (PSNR) and structural similarity index measure (SSIM).

PSNR estimates the absolute error between the reconstructed image and the original image. It is calculated based on the mean square error (MSE) as follows.

$$\text{PSNR} = 20 \log_{10} \left( \frac{2^p - 1}{\sqrt{\text{MSE}}} \right), \quad (1)$$

where  $p$  is the sample precision. For grayscale images,  $p = 8$ . The  $\text{psnr}()$  function in MATLAB is used for the calculation. Larger PSNR value indicates better representation quality.

On the other hand, SSIM considers the inter-dependence of the pixels that carries important information about the structure of the objects in the image. The measure between two images  $x$  and  $y$  of common size is calculated as follows

$$\text{SSIM}(x, y) = \frac{(2\mu_x\mu_y + C_1)(2\sigma_{xy} + C_2)}{(\mu_x^2 + \mu_y^2 + C_1)(\sigma_x^2 + \sigma_y^2 + C_2)}, \quad (2)$$

where  $\mu_i$  and  $\sigma_i$  are average and variance of  $i$  ( $i = x, y$ ), respectively, and  $\sigma_{xy}$  is the covariance of  $x$  and  $y$ . The  $\text{ssim}()$  function in MATLAB is used for the calculation that also provides the local SSIM map. Larger SSIM value indicates better representation quality.

### 3.2 Comparison results

Fig. 1 shows eight images chosen for this comparison task, all of which are converted into grayscale. The first four images are publicly available from USC-SIPI or MATLAB image folder. The high-resolution brain MR image Fig. 1(5) is one of the slices extracted from a 7-Tesla MRI of the ex vivo human brain at 100-micron resolution by Edlow *et al* [28]. The last three images are provided by the ASU-Mayo Center for Innovative Imaging.

The results for sample density at 3% are shown in Table 1, while those for sample density at 10% are shown in Table 2. It is clear that the representation quality improves when sample density increases because more information is embedded in the measurement data.

For results in each table, that is, at the same sample density, AMA provides the best representation quality in terms of both PSNR and SSIM. ISTA performs the worst in terms of the reconstruction quality, which might be due to the default threshold values used in the code. Finding optimal values for the parameters could improve the performance. However, this comparison results deliver an overall message that AMA representation can provide better quality than CS algorithms.

It is interesting to observe that, for the high-resolution brain MR image in Fig. 1(5), TVEq performance is close to that of AMA in terms of both PSNR and SSIM. At the same time, ISTA is also close in terms of SSIM. Similar results are observed for AD (PET) image in Fig. 1(7). The reason might be due to the high sparsity of those two images.

Fig. 2 shows the reconstruction results for image Lena at sample density 10%, and Fig. 3 shows the reconstruction results for image migraine (MRI) at sample density 3%. The results for other images are similar.

Fig. 4 shows the anisotropic triangular meshes for the original images produced by AMA representation at sample density 3%. As can be seen, the triangular elements concentrate around the edges of the images so that they can represent the key features of the images.

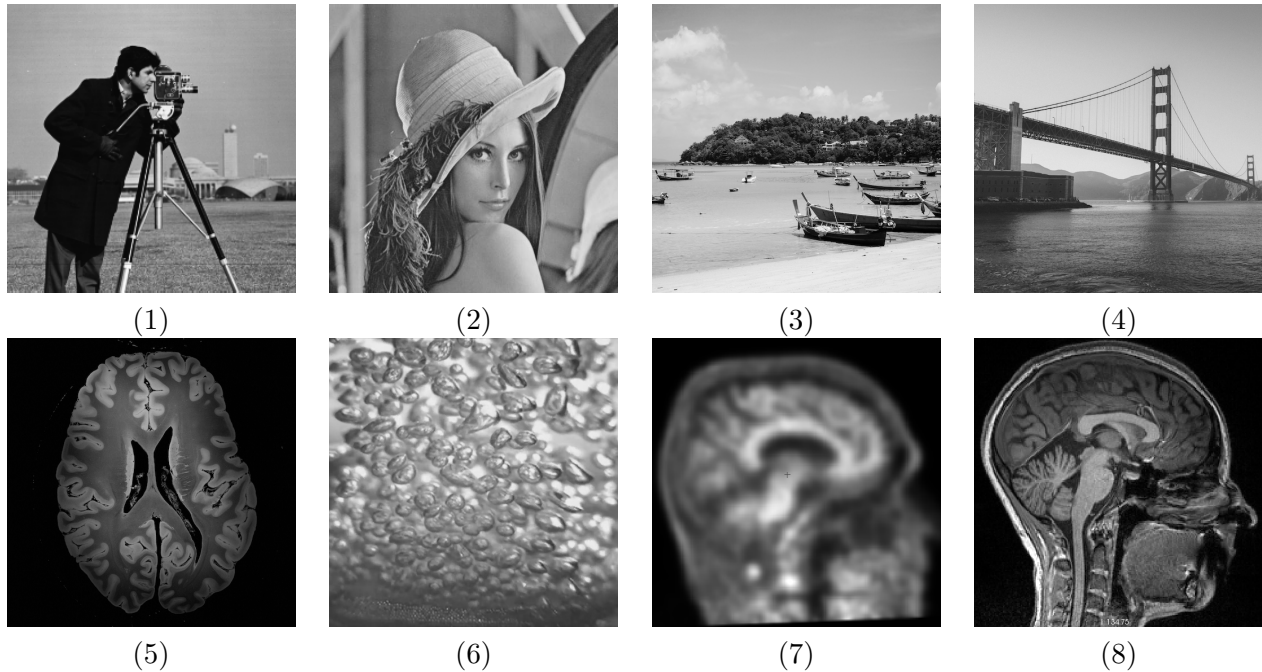


Figure 1: Original images: (1) cameraman,  $256 \times 256$ , (2) Lena,  $512 \times 512$ , (3) beach,  $730 \times 730$ , (4) bridge,  $3000 \times 3000$ , (5) brain MRI,  $1760 \times 1760$ , (6) heat bubble,  $720 \times 720$ , (7) AD (PET),  $960 \times 960$ , and (8) migraine (MRI),  $960 \times 960$ .

Table 1: Comparison of representation qualities at sample density 3%

image	resolution	PSNR (dB)			SSIM		
		TVec	ISTA	AMA	TVec	ISTA	AMA
cameraman	$256 \times 256$	30.69	18.90	33.09	0.61	0.54	0.74
Lena	$512 \times 512$	31.98	23.59	35.23	0.74	0.69	0.85
beach	$730 \times 730$	32.82	21.35	35.04	0.75	0.69	0.83
bridge	$3000 \times 3000$	34.91	27.31	36.92	0.80	0.74	0.85
brain MRI	$1760 \times 1760$	35.38	28.24	36.15	0.68	0.65	0.71
heat bubble*	$720 \times 720$	30.80	25.23	34.91	0.73	0.77	0.87
AD (PET)*	$960 \times 960$	40.82	38.53	44.49	0.94	0.95	0.96
migraine (MRI)*	$960 \times 960$	32.08	24.27	34.09	0.69	0.68	0.78

(\*: provided by ASU-Mayo Center for Innovative Imaging.)

## 4 Conclusions

In this paper, we have performed a preliminary comparison between compressive sampling and adaptive sampling, specifically, AMA representation. Due to the large number of methods developed in the CS field, this comparison is by no means thorough. However, the work does provide some guidance for future efforts in the area of image representation.

Our results indicate that AMA representation can provide better representation quality than CS algorithms. CS works well for ideal sparse signals but may not for natural images. Although different

Table 2: Comparison of representation qualities at sample density 10%

image	resolution	PSNR (dB)			SSIM		
		TVeq	ISTA	AMA	TVeq	ISTA	AMA
cameraman	$256 \times 256$	32.29	21.21	34.44	0.73	0.66	0.82
Lena	$512 \times 512$	34.51	27.26	38.22	0.84	0.80	0.92
beach	$730 \times 730$	34.28	23.68	36.59	0.81	0.78	0.90
bridge	$3000 \times 3000$	37.58	30.86	40.50	0.87	0.82	0.92
brain MRI	$1760 \times 1760$	36.09	30.05	36.84	0.72	0.70	0.74
heat bubble*	$720 \times 720$	34.43	31.34	40.94	0.87	0.89	0.96
AD (PET)*	$960 \times 960$	47.59	40.23	47.36	0.98	0.96	0.98
migraine (MRI)*	$960 \times 960$	35.41	26.94	36.21	0.84	0.77	0.87

(\*: provided by ASU-Mayo Center for Innovative Imaging.)

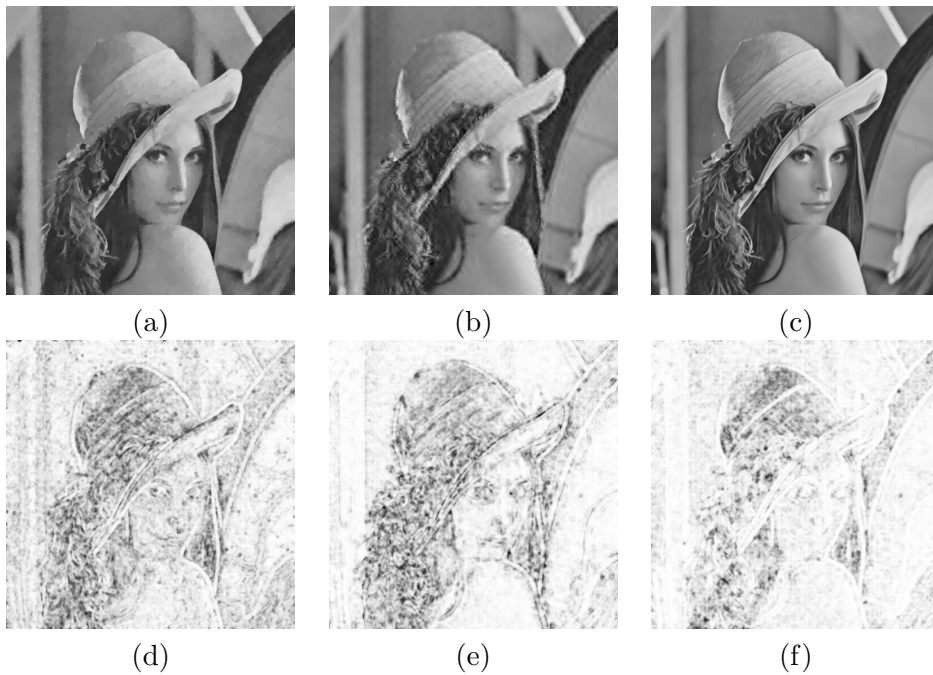


Figure 2: Reconstruction of image Lena at sample density 10%: (a) TVeq, PSNR=34.51, (b) ISTA, PSNR=27.26, (c) AMA, PSNR=38.22, (d) TVeq SSIM map, SSIM=0.84, (e) ISTA SSIM map, SSIM=0.80, and (f) AMA SSIM map, SSIM=0.92.

measurement matrix can be designed, and various parameter values in different algorithms can be optimized, the improvement of CS performance, especially on natural images, may still be modest. Further comparison with recently developed CS algorithms is needed.

On the other hand, AMA representation works directly on image pixels by performing anisotropic mesh adaptation to concentrate triangular elements around the edges of the images. Although some parameters are used for the mesh adaptation procedure, their default values in the program code work well for general problems. The representation procedure is straightforward without the need to specify different parameters other than the desired sample density. Note that the AMA representation quality

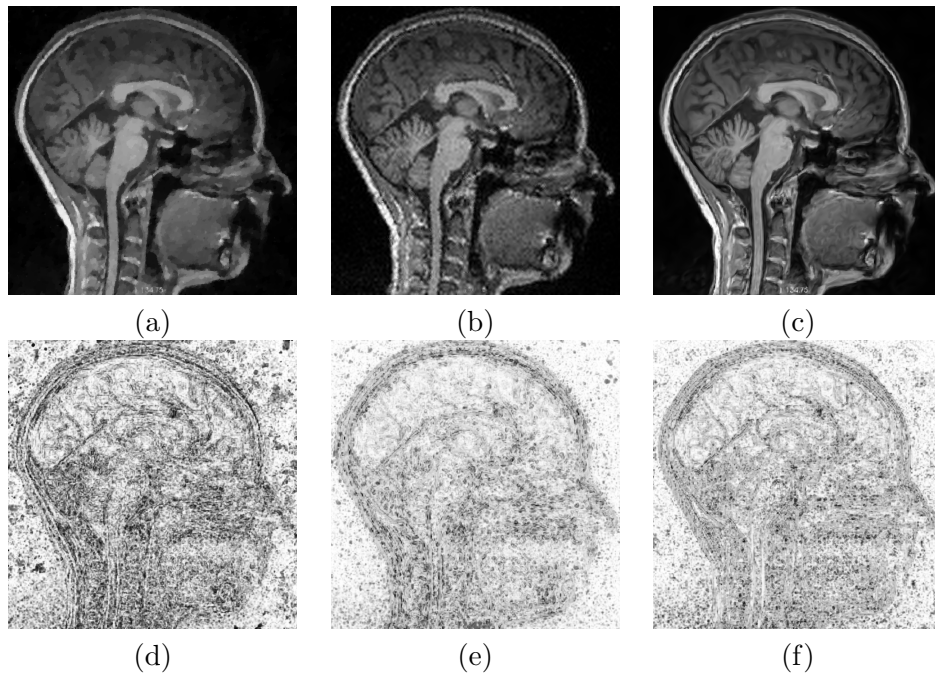


Figure 3: Reconstruction of image migraine (MRI) at sample density 3%: (a) TVeq, PSNR=32.08, (b) ISTA, PSNR=24.27, (c) AMA, PSNR=34.09, (d) TVeq SSIM map, SSIM=0.69, (e) ISTA SSIM map, SSIM=0.68, and (f) AMA SSIM map, SSIM=0.78.

can still be improved by adopting the greedy-point-removal algorithm (GPRAMA) at the expense of more computational cost.

Besides better representation quality than compressive sampling, AMA representation can also be applied to improve the efficiency of partial differential equation based image processing such as image segmentation.

## References

- [1] Candes, E.J., Romberg, J., Tao, T.: Robust uncertainty principles: exact signal reconstruction from highly incomplete frequency information. *IEEE Transactions on Information Theory*, 52(2), 489-509, (2006).
- [2] Donoho, D.L.: Compressed sensing. *IEEE Transactions on Information Theory*, 52(4), 1289-1306, (2006).
- [3] Chartrand, R.: Exact reconstructions of sparse signals via nonconvex minimization. *IEEE Signal Processing Letters*, 14(10), 707-710, (2007).
- [4] Donoho, D.L. and Tsaig, Y.: Fast solution of l1-norm minimization problems when the solution may be sparse. *IEEE Transactions on Information Theory*, 54(11), 4789-4812, (2008).
- [5] Blumensath, T. and Davies, M.: Iterative thresholding for sparse approximations. *Journal of Fourier Analysis and Applications*, 14, 629-654, (2008).

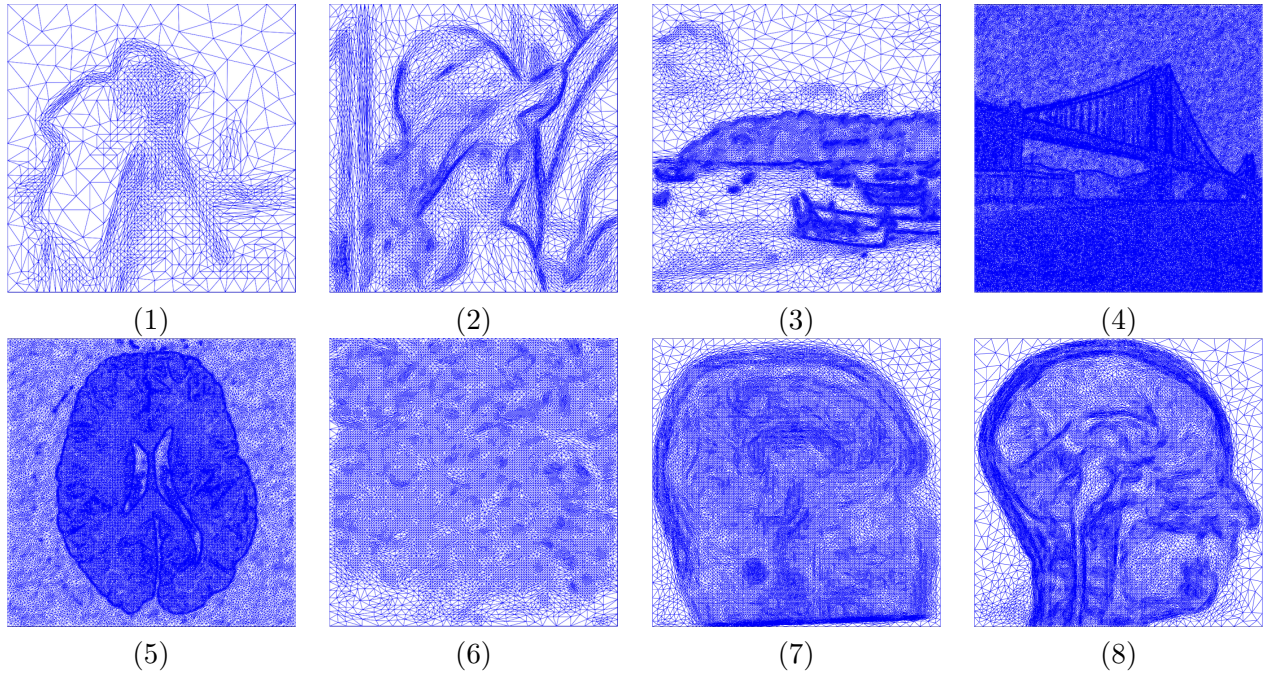


Figure 4: Anisotropic triangular meshes for AMA representation at sample density  $\frac{1}{3}$ : (1) camera-man, (2) Lena, (3) beach, (4) bridge, (5) brain MRI, (6) heat bubble, (7) AD (PET), and (8) migraine (MRI).

- [6] Dai, W. and Milenkovic, O.: Subspace pursuit for compressive sensing signal reconstruction. *IEEE Transactions on Information Theory*, 55(5), 2230 - 2249, (2009).
- [7] Needel, D. and Vershynin, R.: Signal recovery from incomplete and inaccurate measurements via regularized orthogonal matching pursuit. *IEEE Journal of Selected Topics in Signal Processing*, 4(2), 310-316, (2010).
- [8] Kovarik, L., Stevens, A., Liyu, A. and Browning, N.D.: Implementing an accurate and rapid sparse sampling approach for low-dose atomic resolution STEM imaging. *Applied Physics Letters*. 109(16), 164102, (2016).
- [9] Tian, Z., Jia, X., Yuan, K., Pan, T. and Jiang, S.B.: Low-dose CT reconstruction via edge preserving total variation regularization. *Phys Med Biol*. 56(18): 5949–5967, (2011).
- [10] Li, X. and Luo, S.: A compressed sensing-based iterative algorithm for CT reconstruction and its possible application to phase contrast imaging. *BioMedical Engineering OnLine*, 10:73, (2011).
- [11] Lustig, M.: Sparse MRI: the application of compressed sensing for rapid MR imaging. *Magnetic Resonance in Medicine*, 58(6), 1182–1195, (2007).
- [12] Lustig, M., Donoho, D.L., Santos, J.M. and Pauly, J.M.: Compressed sensing MRI. *IEEE Signal Processing Magazine*, 25(2), 72–82, (2008).
- [13] Tashan, T. and Al-Azawi, M.: Multilevel magnetic resonance imaging compression using compressive sensing. *IET Image Processing*, 12(12), 2186–2191, (2018).



- [14] Fei, X., Wei, Z. and Xiao, L.: Iterative directional total variation refinement for compressive sensing image reconstruction. *IEEE Signal Processing Letters*. 20(11), 1070–1073, (2013).
- [15] Liu, L., Xie, Z., and Feng, J.: Backtracking-based iterative regularization method for image compressive sensing recovery. *Algorithms*, 10, 1–8, (2017).
- [16] Terzopoulos, D. and Vasilescu, M.: Sampling and reconstruction with adaptive meshes. In *Proceedings of the IEEE Computer Vision and Pattern Recognition Conference (CVPR'91)*, 70–75, (1991).
- [17] Davoine, F., Antonini, M., Chassery, J-M., and Barlaud, M.: Fractal image compression based on Delaunay triangulation and vector quantization. *IEEE Trans. Image Process*, 5(2), 338–346, (1996).
- [18] Ramponi, G. and Carrato, S.: An adaptive irregular sampling algorithm and its application to image coding. *Image Vis. Comput*, 19, 451–460, (2001).
- [19] Yang, Y., Wernick, M.N. and Brankov, J.G.: A fast approach for accurate content-adaptive mesh generation. *IEEE Trans. Image Process*, 12(8), 866–881, (2003).
- [20] Su, D. and Willis, P.: Image interpolation by pixel-level data-dependent triangulation. *Comput. Graph. Forum*, 23(2), 189–201, (2004).
- [21] Brankov, J.G., Yang, Y. and Wernick, M.N.: Tomographic image reconstruction based on a content-adaptive mesh model. *IEEE Trans. Med. Imaging*, 23(2), 202–212, (2004).
- [22] Demaret, L. and Iske, A.: Adaptive image approximation by linear splines over locally optimal Delaunay triangulations. *IEEE Signal Process. Lett.*, 13(5), 281–284, (2006).
- [23] Sarkis, M. and Diepold, K.: Content adaptive mesh representation of images using binary space partitions. *IEEE Trans. Image Process.*, 18(5), 1069–1079, (2009).
- [24] Adams, M.D.: A flexible content-adaptive mesh-generation strategy for image representation. *IEEE Trans. Image Process.*, 20(9), 2414–2427, (2011).
- [25] Li, X.: Anisotropic mesh adaptation for image representation. *EURASIP Journal on Image and Video Processing*, 2016:26, (2016).
- [26] Candes, E. and Romberg, J.: L1-MAGIC. <https://statweb.stanford.edu/~candes/software/l1magic/>, last accessed on 11/15/2020.
- [27] Kliesch, M.: pit — Pictures: Iterative Thresholding algorithms. [https://github.com/MartKl/CS\\_image\\_recovery\\_demo](https://github.com/MartKl/CS_image_recovery_demo), last accessed on 11/15/2020.
- [28] Edlow, B.L., Mareyam, A., Horn, A. et al.: 7 Tesla MRI of the ex vivo human brain at 100 micron resolution. *Sci Data* 6, 244 (2019). <https://doi.org/10.1038/s41597-019-0254-8>.